Solar Energy Materials and Solar Cells 174 (2018) 370–379

Contents lists available at ScienceDirect

Solar Energy Materials and Solar Cells

journal homepage: www.elsevier.com/locate/solmat

Electronic and optical properties of ultra-thin 2D tungsten disulfide for photovoltaic applications

Sayan Roy*, Peter Bermel

School of Electrical & Computer Engineering, Purdue University, West Lafayette, IN, USA

ARTICLE INFO

Keywords:
Transition metal di-chalcogenides (TMDC)
Tungsten disulfide (WS_2)
Photovoltaics
Solar cell

ABSTRACT

Atomically thin 2D layered semiconductor materials such as Transition Metal Di-Chalcogenides (TMDCs) have great potential for use as flexible, ultra-thin photovoltaic materials in solar cells due to their favorable photon absorption and electronic transport properties. The electronic properties, such as band structure and bandgap, and optical absorption properties of Tungsten Disulfide (WS_2) were obtained from Density Functional Theory (DFT) calculations; the properties of WS_2 make it a favorable photovoltaic material. Using these properties, we have modelled, using numerical calculations and simulations, a solar cell based on monolayer and bulk WS_2 together with amorphous silicon (a-Si). The maximum efficiency of this cell is 23.26% with V_{OC} of 0.843 V and J_{SC} of 33.49 mA/cm^2. The performance of our solar cell is comparable to many commercial cells. The results show how monolayer WS_2 can serve as a suitable photovoltaic material, opening possibilities to develop solar cells based on 2D TMDC materials.

1. Introduction

Two-dimensional (2D) materials have gathered an increasing amount of interest from their unique potential benefits for a wide variety of optoelectronic devices [1–10]. Transition metal di-chalcogenides (TMDCs) are among the most attractive 2D layered materials that can be fabricated with atomic-scale thickness and a significant bandgap, as a replacement for bulk semiconductors for photovoltaic (PV) applications [2,5,8]. Ultra-thin multi-junction structures can be easily stacked due to van der Waals interactions [2,3]. The 2D monolayers of TMDCs have direct band gaps while the bulk structures have indirect bandgap [2,7]. They have promising electronic and optical properties suitable for applications in photovoltaics [1]. It has been reported that 2D TMDC materials can absorb up to 5–10% of incident sunlight in less than 1 nm thickness and can achieve significantly higher sunlight absorption per unit volume than commonly used solar absorbers such as GaAs and Si [11]. This could potentially make for much more lightweight and flexible photovoltaic modules.

Tungsten Disulfide (WS_2), a Transition Metal Di-Chalcogenide (TMDC), is an important 2D layered material which has attracted a great deal of interest because of its significant chemical and physical properties. It has a band gap of 1.3–2.2 eV, well within the range of photovoltaic materials, which makes it attractive for these applications. Its 2D layered structure makes it possible to modify and tune its electronic properties by doping with other atoms or molecules between weakly bonded layers. It is also possible to apply external force to modify its structure, and hence, its electronic properties. Like other TMDCs, WS_2 has significant absorption of incident photons with energies above its bandgap, make it a good absorber. It also exhibits excellent carrier transport properties, as demonstrated by high typical mobility values.

Here, bulk WS_2 was selected as the starting material for designing an initial device. Using this as the baseline, monolayer WS_2 and amorphous silicon (a-Si) were added to improve the performance. The electronic properties of monolayer, bilayer and bulk WS_2 were studied using Density Functional Theory (DFT) calculations, from which the band structures and corresponding bandgaps were obtained. From these calculations, the absorption coefficient for different photon energies was calculated along with other parameters such as the relative dielectric constant, conduction band effective density of states and valence band effective density of states. Using these results, a p-n junction solar cell was modelled and simulated using monolayer WS_2, bulk WS_2 and a-Si to obtain a structure similar to HIT (Heterojunction with Intrinsic Thin Layer) solar cells, which are known to have high efficiencies. The structure was simulated using the drift-diffusion model to obtain the device parameters such as open circuit voltage (V_{OC}), shot circuit current (J_{SC}) and efficiency. The maximum efficiency obtained was 23.26% with V_{OC} of 0.843 V and J_{SC} of 33.49 mA/cm^2. These values compare favorably with the best HIT silicon solar cells observed in experiments, with efficiencies of 25.6% [12].

* Correspondence to: Purdue University, School of Electrical and Computer Engineering, Birck Nanotechnology Center, BRK 2270, 1205 West State St., West Lafayette, IN 47907, USA.
E-mail address: roy1@purdue.edu (S. Roy).

http://dx.doi.org/10.1016/j.solmat.2017.09.011
Received 26 January 2017; Received in revised form 22 June 2017; Accepted 8 September 2017
Available online 25 September 2017
0927-0248/

2. Theory and methods

2.1. Structure of tungsten disulfide (WS_2)

WS_2 has a trigonal prismatic structure where each layer consists of a layer of hexagonally arranged W atoms sandwiched between two layers of hexagonally arranged S atoms [13,14]. The thickness of a single layer of WS_2 is 3.2 Å, while multiple layers are separated from each other by empty space of separation 2.96 Å, and the lattice parameter a is 3.154 Å, as determined by single-crystal electron diffraction [14]. There are strong W-W, S-S and W-S covalent bonds within a layer, while adjacent layers are held together by weak can der Waals' forces. A primitive unit cell consists of one W atom and two S atoms in a trigonal prismatic configuration [13–16].

2.2. Electronic band structure from DFT and GW calculations

Electronic Band Structure is one of the most fundamental properties of a material and is the foundation for understanding its various properties. Density Functional Theory (DFT) was used to obtain the preliminary band structure of WS_2. DFT is a powerful quantum mechanical method to obtain band structure, states and energies of a material using many-body perturbation theory [17,18]. The DFT calculations were performed using the open source code Quantum ESPRESSO [19,20]. Quantum ESPRESSO is a quantum mechanical modelling tool to simulate many-body systems. DFT calculations require pseudopotential files which simulate selected atoms from the periodic table. The pseudopotentials developed for Quantum ESPRESSO were used in our simulations. It is very important to correctly define the unit cell, such as position of atoms, cell dimensions and appropriate pseudopotential files. GGA pseudopotentials (which add gradient correction to the more basic LDA ones), as described by Perdew-Burke-Ernzerhof (PBE) scheme [21], were used to simulate W and S atoms. Since it is a thin 2D structure, there is no electronic dispersion in the vertical out-of-plane direction. Thus, a horizontal sampling in the x-y plane of the first Brillouin zone is sufficient to obtain accurate electronic dispersion. The Brillouin zone was sampled according to the scheme proposed by Monkhorst-Pack [22] with a high-density in-plane $20 \times 20 \times 1$ k-point grid with 400 k-points. The cutoff energy used was 20 Ry. The materials were modelled as cuboidal slabs by including a vacuum region of 20 Å in the direction perpendicular to the surface. The bands were plotted along the k-point path as in Fig. 1 (right, green).

The band structure obtained from DFT gives accurate information about the shape of the energy bands (such as VBM and CBM). But a major problem is that the bandgap of the material is significantly underestimated. A theoretically rigorous way to solve the issue of band gap underestimation is to go beyond the DFT results and formulating the electronic band structure using the GW approximation; it involves the expansion of the self-energy in terms of the single particle Green's function G and the screened Coulomb interaction W to model many-body systems [13,23–26]. The results from DFT calculations were used as the starting point for the GW calculations; the simulations were carried using the GWL package in Quantum ESPRESSO [19,27]. The bandgap energy correction value was obtained from the GW approximation, which when added to the DFT bands gave the accurate band structure of bulk WS_2 matching with experiments [13]. However, for a material of WS_2 consisting of only a few layers, namely monolayer and bilayer, it is important to include the excitonic effect due to the exciton binding energy [28]. The bandgaps of monolayer and bilayer WS_2 obtained by DFT calculations followed by adding the GW corrections are significantly higher than experimental results. The large overestimation in these structures is due to the large excitonic effect in a two-dimensional system. The energy correction due to the excitonic effect when subtracted from the DFT + GW bands gives very accurate band structure and bandgap matching closely with experimental results obtained via spectroscopic ellipsometry and electrochemical cyclic voltammetry [5,28–30].

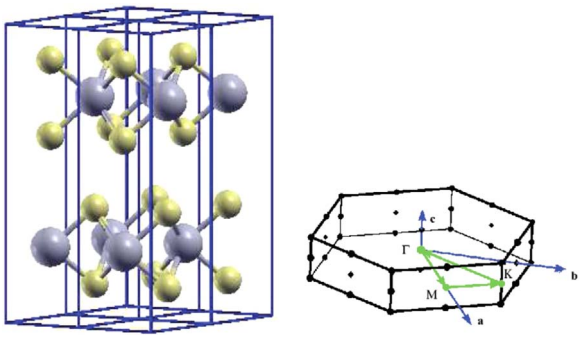

Fig. 1. Left: illustration of the 2Hb-WS_2 structure where the big and small balls represent W and S atoms, respectively. Right: the corresponding Brillouin zone where the **k** path used to plot the band structure diagram is also shown (adapted from [13]).

The DFT calculations and GW approximation were first attempted with silicon to validate our procedure. The results obtained with silicon were comparable to established results. The bandgap of bulk silicon which we obtained from DFT calculations followed by inclusion of GW correction was 1.14 eV, which is very close to the actual bandgap of 1.12 eV [31]. All the calculations and simulations were carried out assuming a temperature of 300 K.

2.3. Absorption coefficient calculation

The band structure and energy data from the DFT results were used in Quantum ESPRESSO to obtain the real and imaginary parts of the dielectric tensor (ε) [32,33]. The calculations were carried out using an energy range of 0–4 eV which covers the energy of visible light and incoming photons in the solar radiation. Increments of 0.01 eV in energy were used in the calculations to obtain accurate results. A thermal broadening of about 0.1 eV was used with the obtained results to obtain realistic results matching with experimental measurements, since it is much easier and more probable to take measurements at increments of 0.1 eV rather than 0.01 eV. The real part of the epsilon data gave the relative dielectric constant of the material. Using the real and imaginary parts of epsilon, the values of the absorption coefficient (α) at the corresponding energies were calculated [34,35]. The plot of the absorption coefficient against energy gave a very clear picture of the photon energies which are most likely to be absorbed by WS_2, and aid in the design of a suitable PV absorber material. The absorption coefficient was calculated for monolayer and bulk WS_2. The absorption coefficient of a-Si was taken from existing literature [36]. We calculated the dielectric permittivity (ε) and absorption coefficient (α) of c-Si using our model and compared it to the literature values to validate our procedure. The results we obtained with silicon were compared with data from the PhotonicsDB tool [37] on nanoHUB [38], which match the Handbook of Optical Constants of Solids [39]; the close match between our results and the literature confirms the validity of our model. All the calculations and simulations were carried out assuming a temperature of 300 K.

2.4. Properties of WS_2 and a-Si

The properties of monolayer WS_2, bulk WS_2 and a-Si are summarized in Table 1. The calculated values of the bandgap and dielectric constant were used for monolayer and bulk WS_2. The electron affinity of bulk WS_2 was taken to be 4.5 eV [40]. It has been seen that when a Transition Metal Di-Chalcogenide (TMDC) monolayer is aligned with bulk material, the conduction band of the monolayer is below the conduction band of the bulk material with a band offset of around 0.2 eV in the conduction band [41]; therefore, the electron affinity of monolayer WS_2 is taken to be 4.7 eV. It has been observed in recent

Table 1
Electronic properties of monolayer WS_2, bulk WS_2 and a-Si used in device simulation.

	Monolayer WS_2	Bulk WS_2	a-Si
Bandgap (eV)	2.15 (direct)	1.29 (indirect)	1.7 (direct)
Electron Affinity (eV)	4.7	4.5	4
Relative Dielectric Constant	5.1	13.4	11.7
Conduction Band Effective Density of States N_C (cm^{-3})	$0.97*10^{19}$	$2.02*10^{19}$	$2.82*10^{19}$
Valence Band Effective Density of States N_V (cm^{-3})	$1.34*10^{19}$	$2.48*10^{19}$	$2.65*10^{19}$
Electron Mobility ($cm^2\,V^{-1}\,s^{-1}$)	200	200	1
Hole Mobility ($cm^2\,V^{-1}\,s^{-1}$)	50	50	0.003

work that the electron mobility of WS_2 can be as high as 234 $cm^2\,V^{-1}\,s^{-1}$ [42,43]. Experimentally prepared WS_2 can exhibit some non-idealities, such as sulfur vacancies, which can lead to various electronic defects and non-ideal behavior. We compensate for such issues by taking conservative values for the carrier lifetimes and mobilities, which are drawn directly from experiments. The electron mobility of WS_2 is taken to be 200 $cm^2\,V^{-1}\,s^{-1}$, while the hole mobility is found to be between one-third and one-fourth of the electron mobility [44], which can be as low as 50 $cm^2\,V^{-1}\,s^{-1}$. Because of this relatively low hole mobility, we utilize a design that sidesteps hole minority carrier transport through the WS_2 layer, in favor of the comparatively higher electron mobility. From the corresponding band structure results, the electron and hole effective masses were calculated from the band structures of monolayer and bulk WS_2, using $\frac{1}{m^*} = \frac{1}{\hbar^2}\frac{\partial^2 E}{\partial k^2}$. These values were then used to calculate the conduction band effective density of states N_C and the valence band effective density of states N_V [45]. The bandgap, electron affinity, relative dielectric constant, N_C and N_V of a-Si were taken from standard literature [46,47]. The electron mobility was taken as 1 $cm^2\,V^{-1}\,s^{-1}$ and the hole mobility was taken as 0.003 $cm^2\,V^{-1}\,s^{-1}$ [48].

2.5. Design of a photovoltaic device

A solar cell was designed with the major concept being a p-n junction which would be able to generate electron-hole pairs from incoming photons in sunlight [49–51]. The current in the solar cell and the voltage across the terminals were calculated using the Drift-Diffusion model [52,53]. The tool ADEPT (A Device Emulation Program and Tool) was used on nanoHUB to simulate our structure [54]. ADEPT is a detailed numerical device simulation code developed at Purdue University. The semiconductor equations, Poisson's equation, and the hole and electron continuity equations (assuming drift-diffusion transport), are solved numerically in 1D, subject to appropriate boundary conditions (an ideal Ohmic contact in our case). It is assumed that there is no surface optical reflection and that all incident sunlight enters the cell. The back surface optical reflector used in some of these designs is assumed to be ideal, so that all incident photons are reflected back into the absorbing layers. The simulation results obtained under these conditions from ADEPT have been shown to match closely with experimental observations of current-voltage relationships in light and dark conditions, as well as external quantum efficiency [55–57]. The devices were simulated using the AM 1.5G solar spectrum [54]; both cases of no back surface optical reflection and full back surface optical reflection were studied. It was assumed that there is no optical reflection from the top surface of the device. The final solar cell device with maximum efficiency was designed using a combination of monolayer WS_2, bulk WS_2 and a-Si.

Clearly, recombination occurs in these structures in experiments, which can be accounted for by using conservative values of the carrier lifetimes in our simulations. Based on prior experimental results in related transition dichalcogenides, the electron and hole lifetimes for all the layers with moderate to high doping were taken as 10 ns, while for intrinsically-doped bulk WS_2 the lifetimes were taken as 100 ns. For the carrier lifetimes, both radiative and non-radiative recombination have been considered. For 2D semiconductor TMDCs like WS_2, the non-radiative electron and hole lifetimes are much higher than radiative lifetimes, which is consistent with their direct bandgaps; thus, it is the radiative lifetime that is dominant in the effective carrier lifetime [58]. The lifetimes used in our simulations account for the radiative recombination of electrons and holes, which is the dominant recombination process. The carrier lifetimes used in our simulations are lower for heavily doped layers than lightly doped layers, since there is a reduction in carrier mobility with increased doping [59].

We have reviewed the literature on high levels of doping in silicon and WS_2 to determine the maximum activated doping levels at room temperature. Several researchers have reported doping levels as high as 10^{20} cm^{-3} in silicon [60–62]. As for WS_2, there has not been nearly as much work regarding its properties, since it is a relatively new material; but it has a lot of properties like MoS_2 (band structure, bandgap, absorption profile, physical properties, etc.), as they belong to the same family of transition-metal disulfides. Doping levels as high as 10^{20} cm^{-3} have been experimentally demonstrated in MoS_2 [63]. This result is also physically plausible, as the density of sulfur atoms in a transition-metal disulfide is $\sim 10^{22}$ cm^{-3}. In fact, it is possible to fabricate a doped MoS_2 structure where as much as 10% of the sulfur atoms are replaced by dopant atoms [64], which would correspond to a doping level of 10^{21} cm^{-3}. Since WS_2 and MoS_2 have similar physical, chemical and electronic properties, this provides evidence that it is possible to have doping levels as high as 10^{20} cm^{-3} in WS_2. Nonetheless, out of an abundance of caution, we use conservative values for the doping levels, with the full understanding that experimental verification is ultimately needed for any assumed level of doping. In this work, we have ensured that the doping in any layer does not exceed the value of N_C or N_V (effective density of states in conduction and valence bands, respectively). With this limitation taken into consideration and incorporation of fully activated donors and acceptors, there will not be any issues with incomplete ionization. If there is any loss of majority carriers from inactivated dopants, the loss can be compensated by injecting a higher concentration of dopants, within limits created by effects like ionized impurity scattering and the Moss-Burstein effect.

We have assumed Ohmic contacts in our simulations. The electron affinities of monolayer WS_2, bulk WS_2 and a-Si are 4.7, 4.5 and 4 eV respectively. The metals of choice should have appropriate work functions to provide a favorable Ohmic contact, with a zero or negative Schottky barrier height. For an n-type semiconductor, the work function of the metal must be close to or smaller than the electron affinity of the semiconductor. For a p-type semiconductor, the work function of the metal must be close to or larger than the sum of the electron affinity and the bandgap energy. For n-type monolayer WS_2 and bulk WS_2, we can have aluminum, chromium or silver as the metal contacts, since they have work functions close to or lower than 4.5 eV. For p-type bulk WS_2, we can potentially use platinum, palladium, tungsten, gold, nickel or cobalt as the metal contacts, since their work functions are above 5 eV. As for p-type a-Si, platinum [65] and titanium/palladium [66] have been experimentally demonstrated to provide Ohmic contacts; there is also potential to use lower cost metals with slightly lower work functions, such as tungsten and cobalt. We have given some examples of metals which can be used in our devices but the list is not exhaustive; any commonly-used metal with an appropriate work function can be used.

3. Results

The initial device we consider is an n^+-p-p^+ homojunction structure made from bulk WS_2. The device is then modified by replacing the top bulk WS_2 layer with monolayer WS_2 to obtain a heterojunction

device with improved performance, since monolayer WS_2 has a higher direct bandgap and better absorption than bulk WS_2. The final device is designed by replacing the bottom bulk WS_2 layer with a-Si to obtain a structure similar to HIT solar cells [67]. Incorporating a-Si in the device improves the performance by creating monotonically increasing conduction and valence bands, which improve carrier separation and electron and hole collection. Monolayer WS_2 and a-Si function as carrier selective contacts, where the electrons are collected at the monolayer WS_2 end and the holes are collected at the a-Si end.

Although one could compare the changes of individual parameters such as layer thickness or material parameters, each individual comparison is not always very informative by itself, because the carrier transport and optical absorption interact in a nonlinear fashion with respect to certain parameters – for example, changing the electron affinity can exponentially decrease electron current. Therefore, we have chosen to optimize three distinctive photovoltaic structures representing distinctive material sets with suitable device architectures.

The DFT simulations of bulk WS_2 using Quantum ESPRESSO gave the initial band structure along the first Brillouin zone, with a bandgap of 0.97 eV. A major limitation of this approach is the value of the bandgap obtained (0.97 eV), which is significantly underestimated relative to experiment. Using the dispersion and energy values obtained from the results of DFT calculation, the GW approximation gave the required energy correction (0.32 eV) to obtain the accurate bandgap. This correction, when added to the DFT results gave the correct bandgap and band structure (Fig. 2) matching with established results [13]. The indirect bandgap of bulk WS_2 was obtained to be 1.29 eV, with direct transition starting around 2.2 eV.

The bandgap of WS_2 is similar to a typical photovoltaic material and makes it a very good candidate for use in a solar cell. The band structure has a few interesting features in addition to the photovoltaically significant band gap. Both indirect and direct optical transitions can occur in this material, depending on the energy of the incoming photon in the incident radiation. The electronic dispersion determines the relative location of the CBMs and VBMs, which correspond directly to the strength of these transitions. Subsequently, the regions where strong photon-electron interactions take place can be understood, and an appropriate structure can be designed.

The band structures of bilayer and monolayer WS_2 were obtained using DFT calculations followed by inclusion of GW corrections and excitonic effects (Figs. 3 and 4 respectively). The bandgap of the bilayer material was found to be 1.42 eV (indirect) from DFT calculations; the GW correction obtained was 0.64 eV which had to be added to the DFT results; and the exciton binding energy was calculated to be 0.42 eV which had to be subtracted from the GW-corrected band structure. Thus, bilayer WS_2 was found to have an indirect bandgap of 1.64 eV, with direct transition possible at 2.13 eV. The bandgap of the monolayer material was found to be 1.91 eV (direct) from DFT calculations; the GW correction obtained was 1.14 eV, which had to be added to the DFT results; and the exciton binding energy was calculated to be 0.9 eV which had to be subtracted from the GW-corrected band structure. Thus, bilayer WS_2 was found to have a direct bandgap of 2.15 eV. Based on the band structures, both monolayer and bilayer WS_2 can be considered suitable photovoltaic materials.

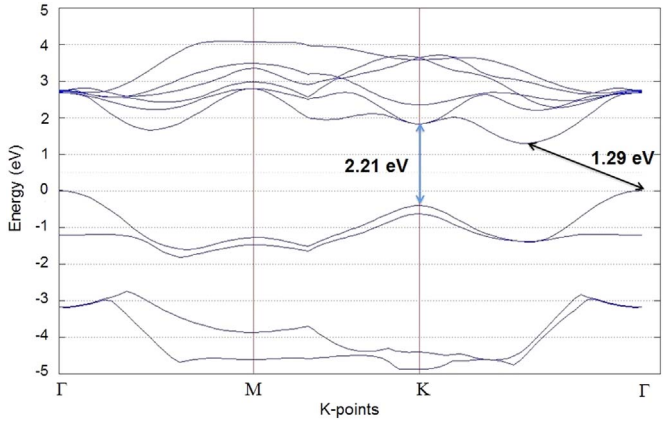

Fig. 2. Band structure of bulk WS_2 showing indirect bandgap of 1.29 eV with direct transition possible at 2.21 eV.

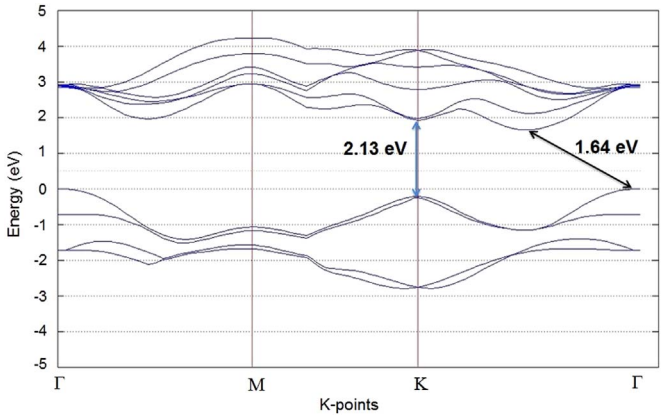

Fig. 3. Band structure of bilayer WS_2 showing indirect bandgap of 1.64 eV with direct transition possible at 2.13 eV.

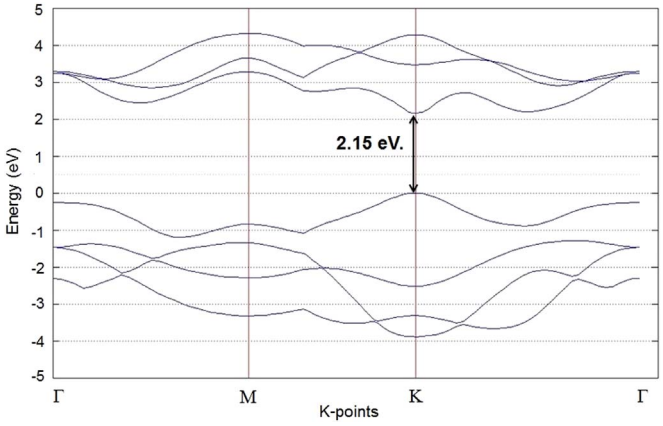

Fig. 4. Band structure of monolayer WS_2 showing direct bandgap of 2.15 eV.

A vacuum spacing of 8 Å between layers was used in the unit cell to obtain the accurate properties of a single 2D monolayer without significant interference from other layers above or below the unit cell. So, a spacing of 8 Å between successive WS_2 layers, where the W and S atoms are aligned in the same vertical axes respectively, can give a thick multi-layer stack of monolayer WS_2. Similarly, a vacuum space of 8 Å between pairs of WS_2 layers was used in the unit cell to obtain the accurate properties of a bilayer structure.

Using the energy eigenvalues and eigenvectors and the dispersion values from the DFT calculations, the real and imaginary parts of the dielectric permittivity ε were obtained for each of the monolayer, bilayer and bulk WS_2 materials. From the dielectric permittivity data, the relative dielectric constant (Table 1) and the value of the absorption coefficient α (μm^{-1}) for different energies of the incoming radiation for monolayer, bilayer and bulk WS_2 (Fig. 5) were obtained. The values of α obtained are similar to values reported in existing literature about WS_2 and similar TMDCs such as Molybdenum Disulfide (MoS_2) [68,69].

The values of α obtained show that there is significant absorption of incoming photons of energies above the direct transition energy value for monolayer, bilayer and bulk WS_2. Bulk WS_2 has decent absorption for photon energies above 2 eV. Bilayer WS_2 has better absorption for photons with similar energies, while monolayer WS_2 has the best absorption profile for photons with energies above 2 eV. Although the

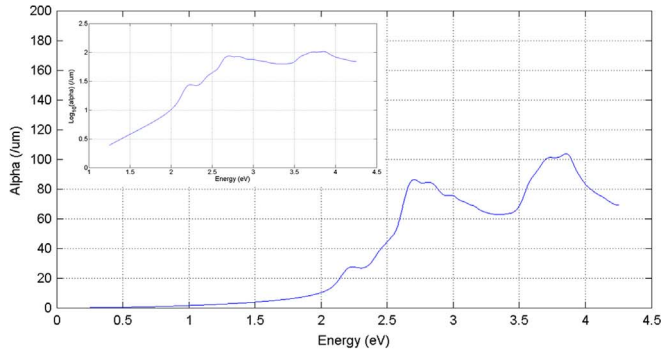

(A) Bulk WS_2

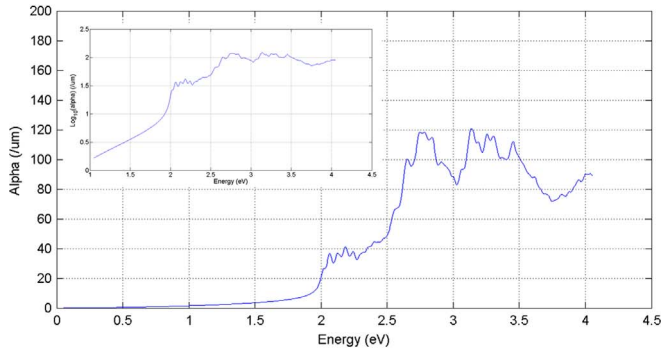

(B) Bilayer WS_2

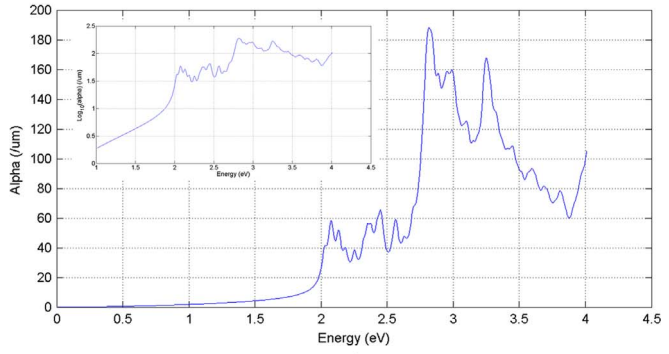

(C) Monolayer WS_2

Fig. 5. Absorption coefficient α (μm^{-1}) vs. energy for monolayer, bilayer and bulk WS_2.

calculated absorption profile shows that there is some absorption for photon energies below the bandgap energy, all sub-bandgap absorption was neglected and the values of alpha for sub-bandgap energies were taken to be zero in our simulations.

Monolayer WS_2 has a direct bandgap of 2.15 eV; bulk WS_2 has an indirect bandgap of 1.3 eV, but a direct transition is possible around 2.2 eV. There is high absorption above the direct transition energy, and very low absorption below that. If we look at the photoluminescence (PL) spectra of WS_2 [70,71], we can observe a spike around the indirect bandgap energy for the bulk material while we see a spike around the direct bandgap energy for the monolayer material. Thus, we can have some photon absorption at the indirect bandgap energy for bulk WS_2, which is why we set its bandgap to be 1.3 eV in our simulations.

For experimental observations, it is evident that there will be some photon absorption for energies between 1.3 eV and 2.2 eV for bulk WS_2 [68,69]. This is our main reason to keep the calculated absorption coefficient values above the indirect bandgap (1.3 eV), and neglect all absorption for energies below this threshold. For monolayer WS_2, any photon absorption below its direct bandgap energy (2.2 eV) is very unlikely, which is why we have used this energy value as its bandgap and neglected all absorption for energies below this threshold.

To design an appropriate solar cell, monolayer and bulk WS_2 were used together with a-Si. The electronic properties of monolayer WS_2, bulk WS_2 and a-Si that were used in the device simulation are summarized in Table 1.

A three-layer junction device was designed to operate as solar cell. The initial structure was an n^+-p-p^+ device designed using only bulk WS_2 for all the three layers. The top layer was a thin layer of highly-doped n-type WS_2; the middle layer was a relatively thick layer of lightly-doped (almost intrinsic) p-type WS_2; and the bottom layer was a thin layer of highly-doped p-type WS_2 [Fig. 6(a)]. We then optimized the layer thicknesses and doping for highest efficiency. The optimal device structure is summarized in Table 2. The open circuit voltage (V_{OC}) for the optimum case was 0.762 V, the short circuit current density (J_{SC}) was 24.14 mA/cm^2, and the efficiency of the solar cell was 15.19%. The significant parameters and features of the solar cell such as short circuit current density (J_{SC}), open circuit voltage (V_{OC}), maximum power voltage (V_{MP}), maximum power current density (J_{MP}), fill factor (FF) and efficiency were recorded for both the cases (Table 3). The band structure, current-voltage (I-V) relationship and external quantum efficiency (EQE) plots for the case of full back surface optical reflection are shown in Fig. 6(b)-(d). The conduction and valence bands are monotonically increasing, which favor carrier collection. It can be seen from the plot of the EQE that there is a significant improvement in carrier generation for wavelengths greater than 0.6 μm, which corresponds to absorption in the space-charge region. The current-voltage relationship shows excellent rectification, which is consistent with a low series and high shunt resistance.

The open circuit voltage (V_{OC}) obtained is similar to that of silicon solar cells [72]; the short circuit current density (J_{SC}) is reasonable for a solar cell, although well below the theoretical limit for the 1.29 eV bandgap of WS_2. While the overall efficiency is not very high, it is promising as a starting point to systematically improve our device. It can be seen that using a perfect back surface optical reflector increases J_{SC} by a significant amount, and improves the performance and efficiency of the device.

The device was then modified by replacing the top bulk WS_2 layer with monolayer WS_2 of same doping type [Fig. 7(a)] to obtain a heterojunction device. Monolayer WS_2 has a direct bandgap and provides a higher bandgap window layer for light absorption at the n^+-p junction. This structure was then re-optimized for the highest efficiency with respect to all the layers' doping and thickness, subject to a monolayer maximum thickness of 10 nm, and a maximal doping of $0.95*10^{19}$ cm^{-3}. The optimal device structure is summarized in Table 4. The performance parameters of the solar cell were recorded for both the cases (Table 5). The band structure, current-voltage (I-V) relationship and external quantum efficiency (EQE) plots for the case of full back surface optical reflection are shown in Fig. 7(b)-(d). The conduction and valence bands are also monotonically increasing in this case, which favor carrier collection. There is an abrupt drop in the bands on the monolayer WS_2 side which helps in improved electron collection. It can be seen from the plot of the EQE that there is a slight improvement in carrier collection for wavelengths between 0.6 μm and the band edge. The introduction of a non-zero slope near the front of the cell also significantly improves carrier collection for wavelengths below 0.6 μm.

In this case, the open circuit voltage (V_{OC}) is 0.774 V and the short circuit current density (J_{SC}) was 32.59 mA/cm^2; the efficiency of the solar cell was 20.481% with a perfect back surface optical reflector. Compared to the homojunction device discussed previously, the open circuit voltage (V_{OC}) improves by about 2%; the short circuit current density (J_{SC}) also greatly increases by about 35%, and is now comparable to that of silicon solar cells. Overall, then, the efficiency of the modified device is about 35% higher than the previous case, which is quite high and comparable to commercial solar cells. The results are very promising, but it is possible to improve the device even further, since there are still losses due to recombination of carriers, unsuitable

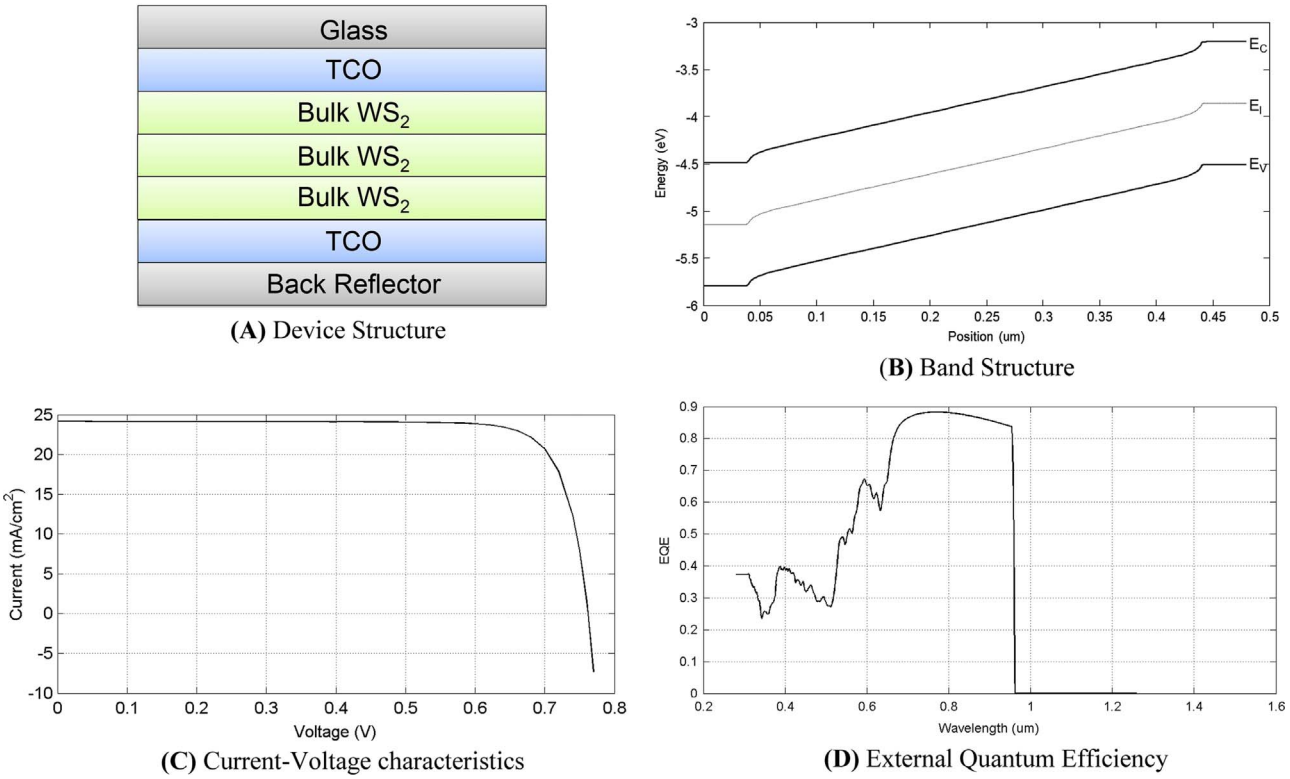

Fig. 6. (A) Device structure; (B) Band structure; (C) I-V plot; and (D) EQE of 3-layer device, using only bulk WS_2 with full back surface optical reflection.

Table 2
Summary of 3-layer device structure using only bulk WS_2.

	Top Layer	Middle Layer	Bottom Layer
Material	Bulk WS_2	Bulk WS_2	Bulk WS_2
Bandgap (eV)	1.29	1.29	1.29
Doping Type	N	P	P
Doping concentration (cm^{-3})	$2*10^{19}$	10^{13}	$2.4*10^{19}$
Thickness (nm)	40	400	40

Table 3
Performance parameters of 3-layer device using only bulk WS_2 (described in Table 2).

	Without Back Surface Optical Reflection	With Full Back Surface Optical Reflection
Open Circuit Voltage V_{OC} (V)	0.760	0.762
Short Circuit Current Density J_{SC} (mA/cm^2)	22.30	24.14
Maximum Power Voltage V_{MP} (V)	0.662	0.665
Maximum Power Current Density J_{MP} (mA/cm^2)	21.09	22.84
Fill Factor FF	0.824	0.826
Efficiency (%)	13.97	15.19

band structure, incomplete absorption, inefficient carrier collection, etc. For instance, the band structure is still non-ideal which penalizes our open circuit voltage by at least 50 mV, and also degrades the short circuit current by at least 1.0 mA/cm^2. Thus, additional modifications will now be investigated to help us approach the Shockley-Queisser limit as closely as possible.

The device was further modified to improve performance by replacing the bottom bulk WS_2 layer with a-Si of same doping type [Fig. 8(a)] to obtain a structure similar to HIT solar cells. Since a-Si has a lower electron affinity than WS_2, it was used to provide a monotonically increasing conduction and valence energy bands so that electrons and holes can easily move towards the opposite contacts and there are no areas in the structure where there could be accumulation of the carriers. a-Si was also used in the structure to prevent recombination of carriers at the back surface contact. This structure was re-optimized with respect to the layers' thicknesses and doping levels. The final device structure with the highest efficiency is summarized in Table 6. The performance parameters of the solar cell were recorded for both the cases (Table 7). The band structure, current-voltage (I-V) relationship and external quantum efficiency (EQE) plots for the case of full back surface optical reflection are shown in Fig. 8(b)-(d). The conduction and valence bands are also monotonically increasing in this case, which provide nearly ideal carrier collection. Also, the abrupt drop in the conduction band on the monolayer WS_2 side which facilitates electron collection, while the abrupt jump in the valence band on the a-Si side improves hole collection. The plot of the EQE is similar to the previous case, with a small improvement near the band edge from a deeper space charge region, resulting in a slightly higher J_{SC}. There is also an improvement in the V_{OC} due to the effect of the back surface field and improved band structure achieved through the introduction of a-Si.

The performance of our final device is found to be much better after incorporating a-Si. The open circuit voltage (V_{OC}) for the best case is 0.843 V and the short circuit current density (J_{SC}) is 33.49 mA/cm^2; the efficiency of the solar cell is 23.26%. The open circuit voltage (V_{OC}) for this cell is much better than the previous structures, and has increased significantly (by about 10% relative, compared to the initial homojunction device); the short circuit current density (J_{SC}) has also increased substantially (by about 38% relative, compared to the initial device). Overall, the efficiency of this solar cell has improved by about 53% relative versus the homojunction device; it is quite high, and comparable to many high-efficiency single junction solar cells [47]. The presence of a perfect back surface optical reflector helps slightly in improving J_{SC}, and thus, the V_{OC}, as well as the overall efficiency of the

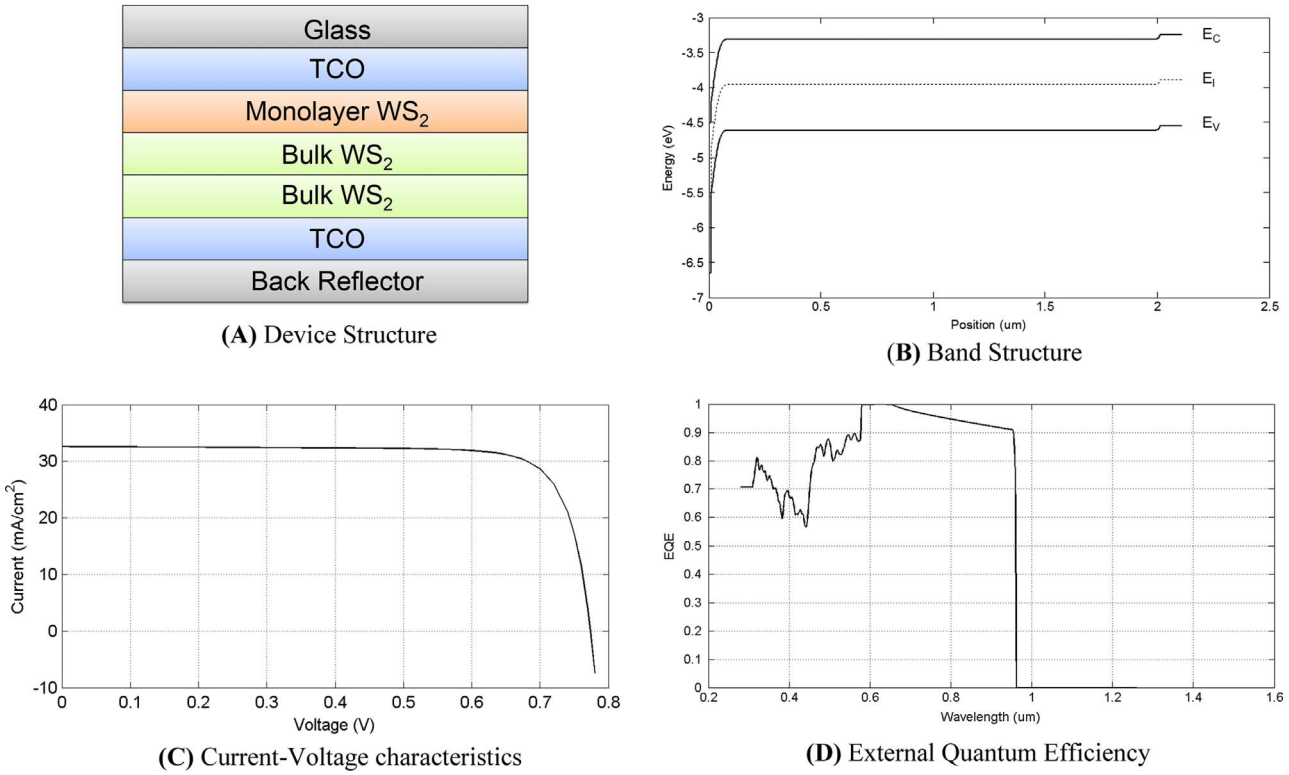

Fig. 7. (A) Device structure; (B) Band structure; (C) I-V plot; and (D) EQE of 3-layer device using bulk and monolayer WS_2 with full back surface optical reflection.

Table 4
Summary of 3-layer device structure using bulk and monolayer WS_2.

	Top Layer	Middle Layer	Bottom Layer
Material	Monolayer WS_2	Bulk WS_2	Bulk WS_2
Bandgap (eV)	2.15 (Direct)	1.29 (Indirect)	1.29 (Indirect)
Doping Type	N	P	P
Doping concentration (cm^{-3})	$0.95*10^{19}$	10^{17}	10^{19}
Thickness (nm)	10	2000	100

Table 5
Performance parameters of 3-layer device using bulk and monolayer WS_2 (structure in Table 4).

	Without Back Surface Optical Reflection	With Full Back Surface Optical Reflection
Open Circuit Voltage V_{OC} (V)	0.774	0.774
Short Circuit Current Density J_{SC} (mA/cm^2)	32.57	32.59
Maximum Power Voltage V_{MP} (V)	0.674	0.674
Maximum Power Current Density J_{MP} (mA/cm^2)	30.38	30.40
Fill Factor FF	0.81	0.81
Efficiency (%)	20.468	20.481

solar cell. These results create new possibilities for the fabrication and use of ultra-thin 2D high-efficiency solar cells using a new material which has the advantages of ultra-low weight per unit of power production, mechanical flexibility, as well as earth abundance, compared to several commonly-used photovoltaic materials.

4. Conclusions and future work

In this work, we have developed a DFT-based model to calculate key materials properties for a Tungsten Disulfide (WS_2) solar cell design, which has been validated against experimentally fabricated and characterized materials. To compensate for expected fabrication impurities and crystal defects, conservative values for parameters such as carrier mobilities and lifetimes are utilized in our device simulations. Using this approach, we find a baseline solar cell design using bulk Tungsten Disulfide (WS_2) gives reasonable performance with an optimal efficiency of around 14%. After making some modifications, such as introducing monolayer WS_2 and a-Si, which improve the band structure and optical performance, the overall efficiency of the optimal solar cell increases significantly to over 23%, which is comparable to the performance of many commercial single-junction solar cells. One key challenge is to obtain high quality a-Si/WS_2 interfaces. It is assumed in this work that crystalline WS_2 is grown on a-Si to best preserve the electronic and chemical properties of the individual components, and to allow efficient carrier transport across the interface [73]. These results show that 2D monolayers of tungsten disulfide (WS_2) have very favorable electronic and optical properties for use in photovoltaics, along with the natural advantages of light weight, flexibility, and earth abundance of most TMDCs.

Nonetheless, WS_2 warrants further investigation, since there are several approaches that could lead to further improvement of performance of our device. For instance, bilayer WS_2 can be used to replace bulk WS_2, since it has a higher bandgap than bulk, but with the same direct transition energy, which implies a higher V_{OC} and comparable J_{SC}. Second, applying a horizontal strain or a vertical compressive force can tune its band structure and bandgap, which can pave the way for a spectrally-adaptable photovoltaic cell, which could also be part of a multi-junction array. Third, the optical reflection implied by the non-ideal External Quantum Efficiency (EQE) of the device can be investigated using various light trapping approaches, such as plasmonics. This approach has yielded methods for guiding and localizing light at

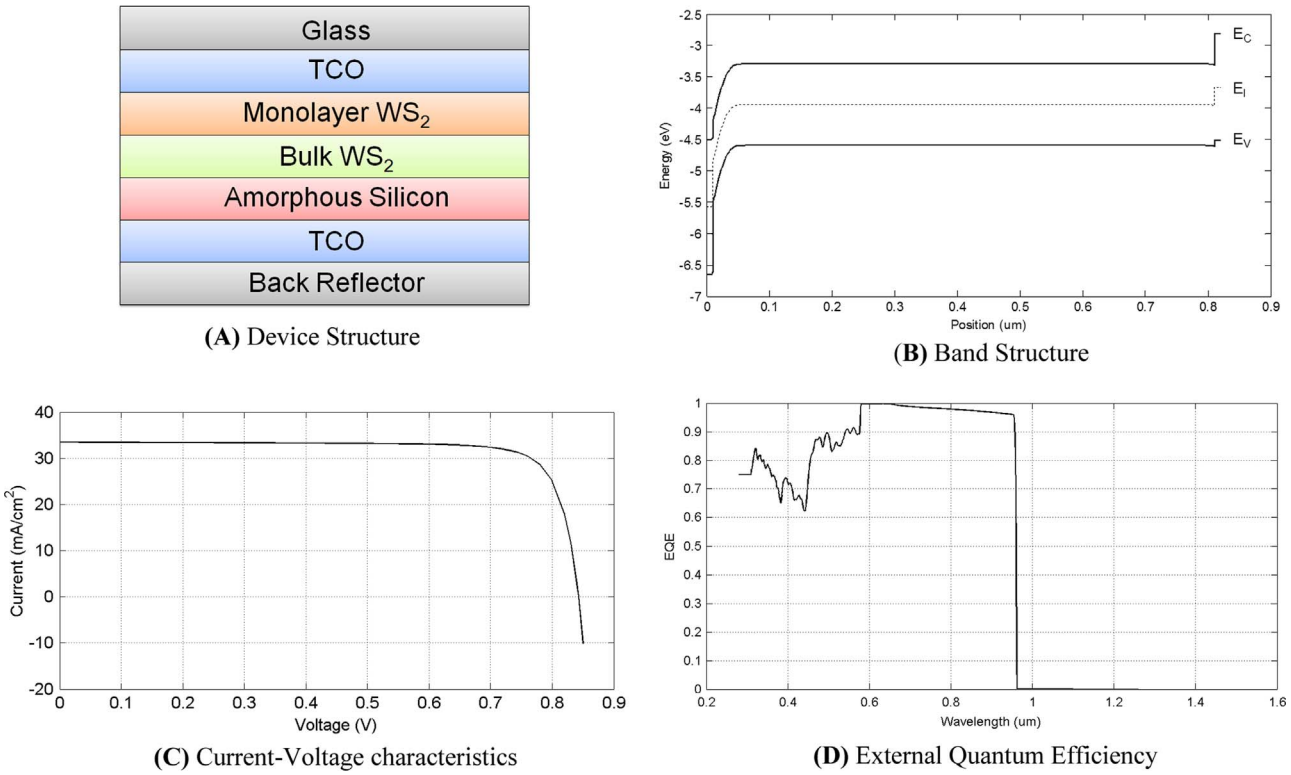

Fig. 8. (A) Device structure; (B) Band structure; (C) I-V plot; and (D) EQE of 3-layer device using bulk WS_2, monolayer WS_2 and a-silicon, with full back surface optical reflection.

Table 6
Summary of 3-layer device structure using bulk WS_2, monolayer WS_2 and a-silicon.

	Top Layer	Middle Layer	Bottom Layer
Material	Monolayer WS_2	Bulk WS_2	a-Si
Bandgap (eV)	2.15 (Direct)	1.29 (Indirect)	1.7 (Direct)
Doping Type	N	P	P
Doping concentration (cm^{-3})	$0.95*10^{19}$	$0.5*10^{18}$	$2.65*10^{19}$
Thickness (nm)	10	800	10

Table 7
Performance parameters of 3-layer device using bulk WS_2, monolayer WS_2 and a-Si (the exact structure is given in Table 6).

	Without Back Surface Optical Reflection	With Full Back Surface Optical Reflection
Open Circuit Voltage V_{OC} (V)	0.842	0.843
Short Circuit Current Density J_{SC} (mA/cm^2)	32.77	33.49
Maximum Power Voltage V_{MP} (V)	0.744	0.745
Maximum Power Current Density J_{MP} (mA/cm^2)	30.54	31.23
Fill Factor FF	0.82	0.82
Efficiency (%)	22.72	23.26

the nanoscale in previous work, allowing for greatly improved absorption in photovoltaic devices [74]. Finally, since we are working with ultra-thin layers, it might be beneficial and more accurate to go beyond the semi-classical drift-diffusion model, and look at quantum effects such as ballistic transport to better understand electron transport and photon absorption at the atomic level.

As far as experimental validation of the optimized design goes, the full device structure should have a back surface optical reflector, such as a screen-printed metal with an appropriate work function as the first layer from the bottom [75]. On top of that, there should be a layer of TCO (Transparent Conducting Oxide), such as ITO (Indium Tin Oxide), of appropriate thickness. The TCO layer is used to collect the free carriers generated in our solar cell. On top of the TCO would be our three-layer structure, which would be covered by another layer of TCO with an anti-reflection coating to collect the generated carriers and allow transmission of incoming solar radiation with minimal surface optical reflection. A layer of glass can be placed as the top layer to protect the inner layers from environmental impurities and disturbances. The monolayer WS_2 layer needs to be prepared such that multiple layers can be stacked together with appropriate interlayer spacing which preserves the electronic properties of monolayer WS_2 [16]. Since Tungsten Disulfide (WS_2) has properties similar to Molybdenum Disulfide (MoS_2), similar dopants can be used in our device, such as alkali metals (Na, K, etc.) in place of tungsten atom (W) as p-type dopants and halogen atoms (Cl, F, etc.) in place of sulfur atoms (S) as n-type dopants [76]. In conclusion, there is a great deal of work yet to be performed on this emerging 2D materials system, but the work to date presented in this paper provides specific predictions based on first principles to help guide further theoretical and experimental investigations.

Funding

The Department of Energy (DOE) (DE-EE0004946) (PVMI Bay Area PV Consortium); NSF Award (EEC-1454315) - CAREER: Thermophotonics for Efficient Harvesting of Waste Heat as Electricity; The Network of Computational Nanotechnology (NSF) (EEC-0228390)

Acknowledgments

The authors thank Jesse Maassen, David Guzman, Xufeng Wang, Mohammad Ryyan Khan and Raghu Chavali for valuable discussions.

References

[1] Q.H. Wang, K. Kalantar-Zadeh, A. Kis, J.N. Coleman, M.S. Strano, Electronics and optoelectronics of two-dimensional transition metal dichalcogenides, Nat. Nanotechnol. 7 (2012) 699–712.

[2] S.M. Auerbach, K.A. Carrado, P.K. Dutta, Handbook of Layered Materials, CRC Press, 2004.

[3] J.P. Wilcoxon, P.P. Newcomer, G.A. Samara, Synthesis and optical properties of MoS2 and isomorphous nanoclusters in the quantum confinement regime, J. Appl. Phys. 81 (12) (1997) 7934–7944.

[4] B.L. Abrams, J.P. Wilcoxon, Nanosize semiconductors for photooxidation, Crit. Rev. Solid State Mater. Sci. 30 (3) (2005) 153–182.

[5] K.F. Mak, C. Lee, J. Hone, J. Shan, T.F. Heinz, Atomically thin MoS2: a new direct-gap semiconductor, Phys. Rev. Lett. 105 (13) (2010) 136805.

[6] A. Ramasubramaniam, D. Naveh, E. Towe, Tunable band gaps in bilayer transition-metal dichalcogenides, Phys. Rev. B 84 (20) (2011) 205325.

[7] R. Coehoorn, C. Haas, J. Dijkstra, C.J.F. Flipse, R.A. de Groot, A. Wold, Electronic structure of MoSe2, MoS2, and WSe2. I. Band-structure calculations and photo-electron spectroscopy, Phys. Rev. B 35 (12) (1985) 6195–6202.

[8] B. Radisavljevic, A. Radenovic, J. Brivio, V. Giacometti, A. Kis, Single-layer MoS2 transistors, Nat. Nanotechnol. 6 (2011) 147–150.

[9] W. Zhang, C.P. Chu, J.K. Huang, C.H. Chen, M.L. Tsai, Y.H. Chang, C.T. Liang, Y.Z. Chen, Y.L. Chueh, J.H. He, M.Y. Chou, L.J. Li, Ultrahigh-gain photodetectors based on atomically thin graphene–MoS2 heterostructures, Sci. Rep. 4 (2014) 3826.

[10] A. Splendiani, L. Sun, Y. Zhang, T. Li, J. Kim, C.Y. Chim, G. Galli, F. Wang, Emerging photoluminescence in monolayer MoS2, Nano Lett. 10 (4) (2010) 1271–1275.

[11] M. Bernardi, M. Palummo, J.C. Grossman, Extraordinary sunlight absorption and one nanometer thick photovoltaics using two-dimensional monolayer materials, Nano Lett. 13 (8) (2013) 3664–3670.

[12] K. Masuko, M. Shigematsu, T. Hashiguchi, D. Fujishima, M. Kai, N. Yoshimura, T. Yamaguchi, Y. Ichihashi, T. Mishima, N. Matsubara, T. Yamanishi, Achievement of more than 25% conversion efficiency with crystalline silicon heterojunction solar cell, IEEE J. Photovolt. 4 (6) (2014) 1433–1435.

[13] H. Jiang, Electronic band structures of molybdenum and tungsten dichalcogenides by the GW approach, Phys. Chem. C 116 (14) (2012) 7664–7671.

[14] R. Tenne, L. Margulis, M.E. Genut, G. Hodes, Polyhedral and cylindrical structures of tungsten disulphide, Nature 360 (1992) 444–446.

[15] W.J. Schutte, J.L. De Boer, F. Jellinek, Crystal structures of tungsten disulfide and diselenide, J. Solid State Chem. 70 (2) (1987) 207–209.

[16] J.A. Wilson, A.D. Yoffe, The transition metal dichalcogenides discussion and interpretation of the observed optical, electrical and structural properties, Adv. Phys. 18 (73) (1969) 193–335.

[17] N.M. Harrison, An introduction to density functional theory, ⟨https://www.ch.ic.ac.uk/harrison/Teaching/DFT_NATO.pdf⟩ (Accessed 31 October 2016).

[18] J.C. Cuevas, Introduction to density functional theory, ⟨https://www.uam.es/personal_pdi/ciencias/jcuevas/Talks/JC-Cuevas-DFT.pdf⟩ (Accessed 31 October 2016).

[19] P. Giannozzi, S. Baroni, N. Bonini, M. Calandra, R. Car, C. Cavazzoni, D. Ceresoli, G.L. Chiarotti, M. Cococcioni, I. Dabo, A. Dal Corso, S. de Gironcoli, S. Fabris, G. Fratesi, R. Gebauer, U. Gerstmann, C. Gougoussis, A. Kokalj, M. Lazzeri, L. Martin-Samos, N. Marzari, F. Mauri, R. Mazzarello, S. Paolini, A. Pasquarello, L. Paulatto, C. Sbraccia, S. Scandolo, G. Sclauzero, A.P. Seitsonen, A. Smogunov, P. Umari, R.M. Wentzcovitch, QUANTUM ESPRESSO: a modular and open-source software project for quantum simulations of materials, J. Phys. Condens. Mater. 21 (39) (2009) 395502.

[20] W. Zhao, R.M. Ribeiro, M. Toh, A. Carvalho, C. Kloc, A.H. Castro Neto, G. Eda, Origin of indirect optical transitions in few-layer MoS2, WS2, and WSe2, Nano Lett. 13 (11) (2013) 5627–5634.

[21] J.P. Perdew, K. Burke, M. Ernzerhof, Generalized gradient approximation made simple, Phys. Rev. Lett. 77 (1996) 3865–3868.

[22] H.J. Monkhorst, J.D. Pack, Special points for Brillouin-zone integrations, Phys. Rev. B 13 (12) (1976) 5188–5192.

[23] F. Aryasetiawan, O. Gunnarsson, The GW method, Rep. Prog. Phys. 61 (1998) 237–312.

[24] F. Bruneval, The GW approximation, ⟨http://www.tddft.org/bmg/files/seminarios/127407.pdf⟩ (Accessed 31 October 2016).

[25] Paolo Umari, Introduction to the GW method, ⟨http://www.quantum-espresso.org/wp-content/uploads/2013/06/talk_school_shanghai13.pdf⟩ (Accessed 31 October 2016).

[26] GWL Manual, ⟨http://www.gwl-code.org/manual_gwl.pdf⟩ (Accessed 31 October 2016).

[27] C. Espejo, T. Rangel, A.H. Romero, X. Gonze, G.M. Rignanese, Band structure tunability in MoS2 under interlayer compression: a DFT and GW study, Phys. Rev. B 87 (24) (2013) 245114.

[28] T. Cheiwchanchamnangij, W.R. Lambrecht, Quasiparticle band structure calculation of monolayer, bilayer, and bulk MoS2, Phys. Rev. B 85 (20) (2012) 205302.

[29] A.R. Beal, H.P. Hughes, Kramers-Kronig analysis of the reflectivity spectra of 2H-MoS2, 2H-MoSe2 and 2H-MoTe2, J. Phys. C: Sol. State Phys. 12 (5) (1979) 881.

[30] J.A. Baglio, G.S. Calabrese, E. Kamieniecki, R. Kershaw, C.P. Kubiak, A.J. Ricco, A. Wold, M.S. Wrighton, G.D. Zoski, Characterization of n-type semiconducting tungsten disulfide photoanodes in aqueous and nonaqueous electrolyte solutions photo-oxidation of halides with high efficiency, J. Electrochem. Soc. 129 (7) (1982) 1461–1472.

[31] C. Kittel, Introduction to Solid State Physics, 6th ed., John Wiley, 1986, p. 185.

[32] R. Ribeiro, Notes on Quantum ESPRESSO, ⟨http://hawk.fisica.uminho.pt/ricardo-ribeiro/QEnotes.html⟩ (Accessed 31 October 2016).

[33] Andrea Benassi, epsilon.x manual, ⟨http://www.quantum-espresso.org/wp-content/uploads/Doc/pp_user_guide.pdf⟩ (Accessed 31 October 2016).

[34] M.S. Dresselhaus, Optical properties of solids, ⟨http://web.mit.edu/6.732/www/opt.pdf⟩ (Accessed 31 October 2016).

[35] E.Y. Tsymbal, Optical properties of solids, ⟨http://unlcms.unl.edu/cas/physics/tsymbal/teaching/SSP-927/Section%2013_Optical_Properties_of_Solids.pdf⟩ (Accessed 31 October 2016).

[36] (a) E.D. Palik, Handbook of optical constants of solids, J. Non-Cryst. Solids 35/36 (1980) 447 (Based on G. Weiser et al.);
(b) P.J. Zanzucchi, C.R. Wronski, D.E. Carlson, J. Appl. Phys. 48 (1977) 5227.

[37] N. Xingjie, L. Zhengtong, A.V. Kildishev, PhotonicsDB: optical constants, ⟨https://nanohub.org/resources/PhotonicsDB⟩, 2015.

[38] nanoHUB, ⟨https://nanohub.org⟩ (Accessed 31 October 2016).

[39] E.D. Palik, Handbook of Optical Constants of Solids, Academic Press, 1997.

[40] S.H. Lee, D. Lee, W.S. Hwang, E. Hwang, D. Jena, W.J. Yoo, High-performance photocurrent generation from two-dimensional WS2 field-effect transistors, Appl. Phys. Lett. 104 (19) (2014) 193113.

[41] S.L. Howell, D. Jariwala, C.C. Wu, K.S. Chen, V.K. Sangwan, J. Kang, T.J. Marks, M.C. Hersam, L.J. Lauhon, Investigation of band-offsets at monolayer–multilayer MoS2 junctions by scanning photocurrent microscopy, Nano Lett. 15 (4) (2015) 2278–2284.

[42] X. Liu, J. Hu, C. Yue, N. Della Fera, Y. Ling, Z. Mao, J. Wei, High performance field-effect transistor based on multilayer tungsten disulfide, ACS Nano 8 (10) (2014) 10396–10402.

[43] M.W. Iqbal, M.Z. Iqbal, M.F. Khan, M.A. Shehzad, Y. Seo, J.H. Park, C. Hwang, J. Eom, High-mobility and air-stable single-layer WS2 field-effect transistors sandwiched between chemical vapor deposition-grown hexagonal BN films, Sci. Rep. 5 (2015) 10699.

[44] R.F. Pierret, G.W. Neudeck, Advanced Semiconductor Fundamentals, 6 Addison-Wesley, 1987 (6.1.3).

[45] R.F. Pierret, G.W. Neudeck, Advanced Semiconductor Fundamentals, 6 Addison-Wesley, 1987, p. 4.

[46] E. Hecht, Optics, 4th edition, Addison Wesley Longman, 2002.

[47] S.M. Sze, K.M. Kwok, Physics of semiconductor devices, 3rd edition, Wiley Online Library, 2007.

[48] E.A. Schiff, Carrier drift-mobilities and solar cell models for amorphous and nanocrystalline silicon, amorphous and polycrystalline thin-film silicon science and technology, Mater. Res. Soc. Symp. Proc 1153 (2009) A15–01.

[49] M.A. Green, Photovoltaic principles, Phys. E: Low-Dimens. Syst. Nanostruct. 14 (1) (2002) 11–17.

[50] Solar Cell Central, PN Junctions & Bandgaps. ⟨http://solarcellcentral.com/junction_page.html⟩ (Accessed 31 October 2016).

[51] Photovoltaic Education Network, The photovoltaic effect. ⟨http://pveducation.org/pvcdrom/the-photovoltaic-effect⟩ (Accessed 31 October 2016).

[52] R.F. Pierret, G.W. Neudeck, Advanced Semiconductor Fundamentals, 6 Addison-Wesley, 1987, p. 6.

[53] R.F. Pierret, Semiconductor Device Fundamentals, Addison, 1996, pp. 3.1–3.2.

[54] J.L. Gray, X. Wang, R.V.K. Chavali, X. Sun, A. Kanti, J.R. Wilcox, ADEPT 2.1, ⟨https://nanohub.org/resources/adeptnpt⟩, 2015.

[55] X. Wang, M.R. Khan, J.L. Gray, M.A. Alam, M.S. Lundstrom, Design of GaAs solar cells operating close to the Shockley–Queisser Limit, IEEE J. Photovolt. 3 (2) (2013) 737–744.

[56] Y. Sun, K.H. Montgomery, X. Wang, S. Tomasulo, M.L. Lee, P. Bermel, Modeling wide bandgap GaInP photovoltaic cells for conversion efficiencies up to 16.5%, Photovoltaic Specialist Conference (PVSC), IEEE 42nd (1-6), 2015.

[57] J.E. Moore, C.J. Hages, N.J. Carter, R. Agrawal, J.L. Gray, M.S. Lundstrom, Current-voltage analysis of band tail effects in CZTSSe through numerical simulation, in: Proceedings of IEEE 42nd Photovoltaic Specialist Conference (PVSC), 2015, pp. 1–6.

[58] K.F. Mak, J. Shan, Photonics and optoelectronics of 2D semiconductor transition metal dichalcogenides, Nat. Photonics 10 (4) (2016) 216–226.

[59] The Minority Carrier Lifetime in Silicon Wafer. ⟨http://meroli.web.cern.ch/meroli/Lecture_lifetime.html⟩ (Accessed 26 May 2017).

[60] J.G. Fossum, R.P. Mertens, D.S. Lee, J.F. Nijs, Carrier recombination and lifetime in highly doped silicon, Solid. State Electron. 26 (6) (1983) 569–576.

[61] G. Masetti, M. Severi, S. Solmi, Modeling of carrier mobility against carrier concentration in arsenic-, phosphorus-, and boron-doped silicon, IEEE Trans. Electron Devices 30 (7) (1983) 764–769.

[62] C.D. Ballif, M. Huljić, G. Willeke, A. Hessler-Wyser, Silver thick-film contacts on highly doped n-type silicon emitters: structural and electronic properties of the interface, Appl. Phys. Lett. 82 (12) (2003) 1878–1880.

[63] V.P. Pham, G.Y. Yeom, Recent advances in doping of molybdenum disulfide: industrial applications and future prospects, Adv. Mater. (2016).

[64] Y. Gong, Z. Liu, A.R. Lupini, G. Shi, J. Lin, S. Najmaei, Z. Lin, et al., Band gap engineering and layer-by-layer mapping of selenium-doped molybdenum disulfide, Nano Lett. 14 (2) (2013) 442–449.

[65] J. Hu, M. Ouyang, P. Yang, C.M. Lieber, Controlled growth and electrical properties of heterojunctions of carbon nanotubes and silicon nanowires, Nature 399 (6731) (1999) 48–51.

[66] B. Tian, X. Zheng, T.J. Kempa, Y. Fang, N. Yu, G. Yu, J. Huang, C.M. Lieber, Coaxial silicon nanowires as solar cells and nanoelectronic power sources, Nature 449 (7164) (2007) 885–889.

[67] R.V.K. Chavali, S. Khatavkar, C.V. Kannan, V. Kumar, P.R. Nair, J.L. Gray, M.A. Alam, Multiprobe characterization of inversion charge for self-consistent

parameterization of HIT cells, IEEE J. Photovolt. 5 (3) (2015) 725–735.
[68] S. Alfihed, M. Hossain, A. Alharbi, A. Alyamani, F.H. Alharbi, P.L.D. Grown Polycrystalline, Tungsten disulphide (WS2) films, J. Mater. (2013) 603648.
[69] B.L. Evans, P.A. Young, Optical absorption and dispersion in molybdenum disulphide, Proc. R.Soc. Lond. A: Math. Phys. Eng. Sci. 284 (1398) (1965) 402–422.
[70] W. Zhao, R.M. Ribeiro, M. Toh, A. Carvalho, C. Kloc, A.H. Castro Neto, G. Eda, Origin of indirect optical transitions in few-layer MoS2, WS2, and WSe2, Nano Lett. 13 (11) (2013) 5627–5634.
[71] H.R. Gutiérrez, N. Perea-López, A.L. Elías, A. Berkdemir, B. Wang, R. Lv, F. López-Urías, V.H. Crespi, H. Terrones, M. Terrones, Extraordinary room-temperature photoluminescence in triangular WS2 monolayers, Nano Lett. 13 (8) (2012) 3447–3454.
[72] Photovoltaic Education Network, Solar cell efficiency records. ⟨http://pveducation.org/pvcdrom/appendices/solar-cell-efficiency-results2⟩ (Accessed 31 October 2016).
[73] Z. Huang, C. Wang, Z. Chen, H. Meng, C. Lv, Z. Chen, R. Han, C. Zhang, Tungsten sulfide enhancing solar-driven hydrogen production from silicon nanowires, ACS Appl. Mater. Interfaces 6 (13) (2014) 10408–10414.
[74] H. Chung, K.Y. Jung, P. Bermel, Flexible flux plane simulations of parasitic absorption in nanoplasmonic thin-film silicon solar cells, Opt. Mater. Express 5 (2015) 2054–2068.
[75] A. Ristow, M.M. Hilali, A. Ebong, A. Rohatgi, Screen-printed back surface reflector for light trapping in crystalline silicon solar cells, ⟨http://ucep.gatech.edu/papers/trapping.pdf⟩, 2001.
[76] J.D. Lin, C. Han, F. Wang, R. Wang, D. Xiang, S. Qin, X.A. Zhang, L. Wang, H. Zhang, A.T.S. Wee, W. Chen, Electron-doping-enhanced trion formation in monolayer molybdenum disulfide functionalized with cesium carbonate, ACS Nano 8 (5) (2014) 5323–5329.